34th Annual International Conference of the IEEE EMBS
San Diego, California USA, 28 August - 1 September, 2012

New workflows and algorithms of bone scintigraphy based on SPECT-CT

Peter Bandi, Norbert Zsoter, Andras Wirth, Ulf Luetzen, Thorsten Derlin, Laszlo Papp

Abstract— **Gold standard bone scintigraphy workflow contains acquisition of planar anterior and posterior images and if necessary, additional SPECTs as well. Planar acquisitions are time consuming and not enough for accurately locating hotspots. Current paper proposes a novel workflow for fast whole body bone SPECT scintigraphy. We present a novel stitching method to generate a whole body SPECT based on the SPECT projections. Our stitching method is performed on the projection series not on the reconstructed SPECTs, thus stitching artifacts are greatly reduced. Our workflow does not require any anterior-posterior image pairs, since these images are derived from the reconstructed whole body SPECT automatically. Our stitching method has been validated on real clinical data performed by medical physicians. Results show that our method is very effective for whole body SPECT generations leaving no signs of artifacts. Our workflow required overall 16 minutes to acquire a whole body SPECT which is comparable to the 60 minutes acquisition time required for gold standard techniques including planar images and additional SPECT acquisitions.**

I. INTRODUCTION

Bone scintigraphy is a widely used method in the field of nuclear medicine [1], [2]. Over the years the workflow of bone scintigraphy slowly adapted. At the beginning only two planar images were acquired about the patient from anterior and posterior directions [1], [3]. Unfortunately these image pairs were not enough to accurately localize a finding [3], [4]. After SPECT became available, the above workflow slightly changed. Nowadays multi-modal systems such as SPECT-CT are widely available and used in the field of bone scintigraphy, where CT provides excellent morphological information next to the SPECT [5]. Nevertheless, planar image pairs are still acquired, but are used only for localization. Based on these planar images one may decide to acquire some additional SPECT scans at certain regions of the body that may be the subject of bone cancer [4], [5]. Unfortunately acquiring a whole body planar image pair is very time-consuming (approx. 30-45 min) and can only be used for localization. Furthermore, acquiring a SPECT FOV (Field of View) takes additional time [6]. This way the overall acquisition time may even be an hour.

Since technology is advancing in both sides of hardware (multi-modal systems, more sensitivity, better resolution, etc.) and software (resolution recovery based SPECT reconstruction methods), it seems logical to re-factor the general workflow of bone scintigraphy.

Our idea was to only acquire SPECT-CT images covering the whole range of the body without collecting any additional planar images. Since one SPECT generally takes significant time, we changed the acquisition parameters to collect less projections in less time. We assumed that a modern resolution recovery reconstruction balances the effects caused by the fast acquisitions [7], [8]. We acquired overlapping SPECT FOVs in order to correctly stitch them together. The reason of requiring such an overlap is that in general the sensitivity at the edges of the detectors is less comparing to the center of it.

Our idea was to perform the stitching of the projections, not on the reconstructed SPECT FOVs. Iterative reconstruction methods accurately determine the maximum likelihood of a statistical value even if the sample set is noisy [7], [8]. In our case this meant that if some of the overlapping projections suffered from the presence of artifacts and/or increased amount of noise, the reconstruction itself would decrease this effect by considering all projections. Obviously, we would not have had such a large amount of statistical input for an accurate stitching by working with already reconstructed images.

In order to provide aid for localization during the evaluation, we generated artificial planar anterior and posterior projection images from the reconstructed whole body SPECT image by deriving attenuation information from the corresponding CT.

Our workflow took average 16 minutes (in case of 5 SPECT FOVs) which is comparable to the one hour needed to acquire planar image pairs and some SPECTs.

II. MATERIALS AND METHODS

A. Patient images

We have collected 36 anonymized DICOM studies acquired by Mediso AnyScan SC SPECT/CT multi-modal camera system. The studies contained the SPECT-CT acquisitions, the reconstructed CT and the SPECT projections. The SPECT images were acquired after injecting Tc-99m MDP radiopharmacon. The type of the collimator was LEGP. The resolution of the SPECT projections was 256×256 pixels. One projection took 5 seconds to acquire. Overall 64 projections were acquired for one FOV and generally 2-6 FOVs were collected for a patient.

The detector shape was octagonal having cut corners of a rectangular shape. The overlapping size of the detector views was 40 mm. All overlapping projections were spatially

P. Bandi, N. Zsoter, A. Wirth and L. Papp are with Mediso Medical Imaging Systems Ltd., Baross str. 91-95, H-1047 Budapest, Hungary, peter.bandi@mediso.hu

T. Derlin is with University Clinic Hamburg-Eppendorf, Germany

U. Luetzen is with Department of Nuclear Medicine, UK-SH Campus Kiel, Germany

978-1-4577-1787-1/12/$26.00 ©2012 IEEE

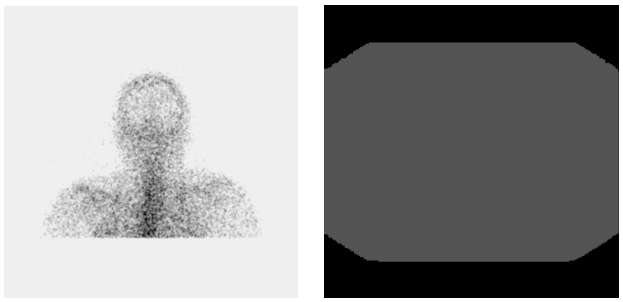

Fig. 1. Left: The first image from a projection series of one SPECT FOV (one bed position). Right: The 2D binary mask created by applying MIP over the projection series.

aligned and this alignment information was derived from the DICOM images, hence no registration was necessary. The average whole body SPECT acquisition took 16 minutes in case of 5 FOVs ($5 * 32 = 160$ seconds / FOV). The CT values were Hounsfield corrected.

B. Methods

1) Stitching: We assumed that the input was a P set of partially overlapping S^p projective SPECT image series of a patient. Each of these series consisted of 2D projective images acquired from different α angles: $S^p = \{S^{p\alpha} | \alpha \in R\}$, where R is the acquisition angle set. The dimensions of the projective images and the acquisition angle set were the same for all S^p series. Spatial and rotational alignment of these images from different series was performed automatically based on DICOM tags.

Empty borders from the images were removed, since the image size was larger than the original field of view.

We obtained the detector shape of the acquisitions from the FOVs in order to perfectly determine the overlapping regions of two sequential SPECT pairs. We focused on this information because we wanted to preserve the background noise distribution on the stitched whole body projection series. In order to determine the shape of the detector we took all projections of the FOVs and performed a maximum intensity projection (MIP) over them. This way we generated a 2D detector mask image.

Let a_{ij} mean the pixel value of A projection at its i^{th} row and j^{th} column. Since the detector shape and size were the same in all $S^{p\alpha} \in S^p$ projections, the mask was obtained by generating a maximum image M^p over the rotations as defined by (1) (see Fig. 1).

$$m_{ij}^p = \max_{\alpha \in A}(s_{ij}^{p\alpha}) \tag{1}$$

where m_{ij}^p and $s_{ij}^{p\alpha}$ is the pixel value of M^p and $S^{p\alpha}$ respectively. This M^p image was threshed at 0 in order to generate a B^p binary mask for all S^p series. The result B^p image had the same size characteristics as any of the $S^{p\alpha}$ images had.

Using the detector mask information we could set up a decision rule of how to choose the final value on the stitched projections. We wanted to avoid stitching methods that operated with derived values, since these methods would change the noise distribution characteristics on the stitched projections. We wanted a kind of fading between the projections, hence we picked one of the overlapping values based on a random variable which depended on the distance of the actual position from the edges of the overlapping area. This way the chance of bringing artifacts to the stitched projections was decreased and the background noise distribution was preserved as well.

Let $S^{p\alpha} \in S^p$ and $S^{q\alpha} \in S^q$ be the overlapping projections acquired from the same α angle with p and q series respectively where $S^p, S^q \in P$. Let the result projection of α acquisition angle be W^α, and the final W is the series of W^α projections from all $\alpha \in R$ angles.

Let $s_{ij}^{p\alpha}$ and $s_{kl}^{q\alpha}$ be the pixel values of $S^{p\alpha}$ and $S^{q\alpha}$ respectively at the same (x, y) spatial position. Assuming that w_{ef}^α is the pixel value of W^α projection at the same (x, y) spatial position, w_{ef}^α is determined as (2).

$$w_{ef}^\alpha = \begin{cases} 0 & \text{if } \neg b_{ij}^p \wedge \neg b_{kl}^q \\ s_{ij}^{p\alpha} & \text{if } b_{ij}^p \wedge \neg b_{kl}^q \\ s_{kl}^{q\alpha} & \text{if } \neg b_{ij}^p \wedge b_{kl}^q \\ DP(s_{ij}^{p\alpha}, s_{kl}^{q\alpha}) & \text{if } b_{ij}^p \wedge b_{kl}^q \end{cases} \tag{2}$$

where $DP(s_{ij}^{p\alpha}, s_{kl}^{q\alpha})$ is defined as (3).

$$DP(s_{ij}^{p\alpha}, s_{kl}^{q\alpha}) = \begin{cases} s_{ij}^{p\alpha} & \text{if } r \in \left[0, {d_p}^\lambda\right) \\ s_{kl}^{q\alpha} & \text{if } r \in \left[{d_p}^\lambda, {d_p}^\lambda + {d_q}^\lambda\right] \end{cases} \tag{3}$$

where d_p and d_q represent the distance of the nearest pixel in vertical direction with 0 value on B^p and B^q respectively, $\lambda \in \mathbb{R}$ is a constant and $r \in \left[0, {d_p}^\lambda + {d_q}^\lambda\right]$ is a random value. Based on initial trials $\lambda = 1.3$ was an appropriate choice. To see a representation of how the stitching is performed between two consecutive projection series, see Fig. 2.

2) Artificial planar A-P image generation: We reconstructed the stitched whole body SPECT projections by applying the OSEMRRAC reconstruction method [7], [8]. The desired reconstructed SPECT axial matrix size was 128×128 with 0.4mm pixel spacing.

The reconstructed CT was resampled and cropped to have the same size as the above SPECT matrix size. The interpolation method for the CT resampling was tri-cubic. This step increased the speed of further CT processing and allowed us to directly calculate attenuation coefficients on the SPECT voxel level.

Multi-threshold was performed on the resampled CT to generate a material map for the attenuation correction. For the threshold intervals used to generate the material map see Tab. I.

The reconstructed whole body SPECT was projected to anterior and posterior direction to generate the artificial planar pairs. During the projection the above CT based material map was used as well. The projection method was

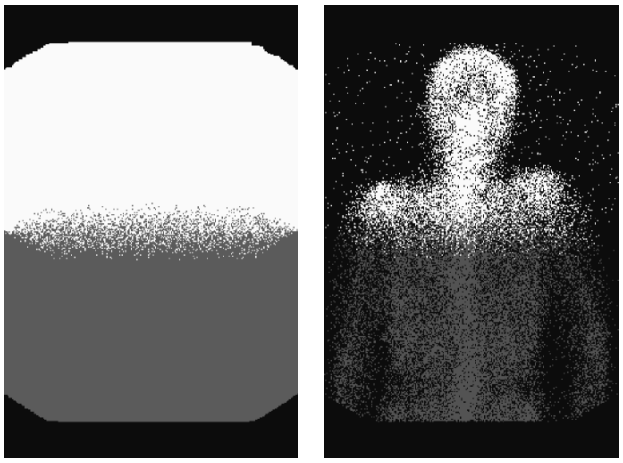

Fig. 2. Left: representation of the result of our stitching method on two consecutive projection series. Different colors indicate the voxel values coming from the bed positions (first bed position = white, second bed position = gray). Right: The same representation on a real clinical acquisition.

TABLE I

TISSUE THRESHOLD INTERVALS AND THEIR RESPECTIVE MATERIAL MAP VALUE

Material	Low threshold	High threshold	Cross-section value
Air	-inf	-400	0.000167
Adipose	-399	20	0.141496
Muscle	21	200	0.158392
Bone	201	inf	0.283790

Where threshold values are considered having Hounsfield units. The cross section values are determined for Tc-99m isotope [9].

performed by considering the cross-section value of the given material (see Tab. I).

We performed an idealistic parallel projection in both anterior and posterior directions through the reconstructed WB SPECT using the material information described in Tab. I. During the calculation of a pixel in the projection images we applied an attenuation model as wefined by eq. 4.

$$y_{ij} = \sum_{k=0}^{n} x_{ikj} e^{-\sum_{s=0}^{k} d\mu_{isj}} \tag{4}$$

where y_{ij} is a pixel value in the given projection image at i, j position, x_{ikj} is the k^{th} voxel value on the projection line of i, j position and d was a constant value representing the reconstructed SPECT voxel size in the coronal direction. μ_{isj} is the macroscopic cross-section of the given material at i, s, j position. For results of an artificial planar anterior and posterior image pair projected from the WB SPECT see Fig. 3.

C. Validation

Validation was based on visual inspection and performed by two medical physicians in Interview Fusion clinical evaluation software developed by Mediso. The validation process covered two main questions: quality of stitching and quality of the artificial planar images.

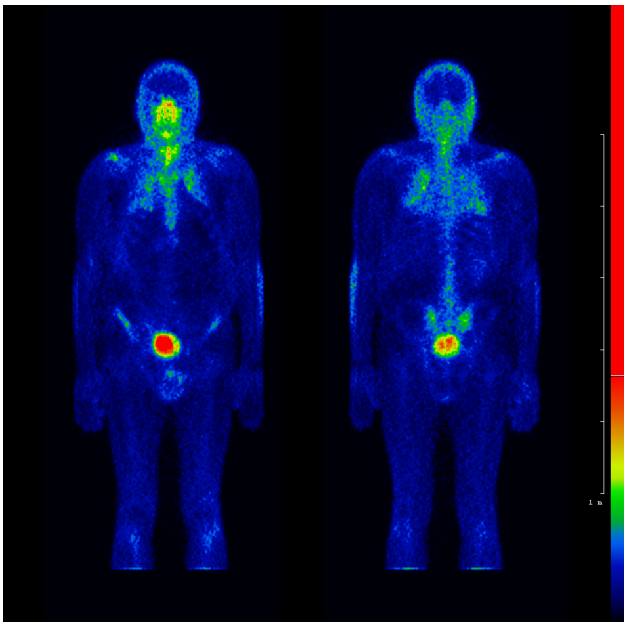

Fig. 3. Artificial planar anterior (left) and posterior (right) image pairs generated from a whole body stitched and reconstructed SPECT. Note that no stitching regions can be discovered on the image pairs.

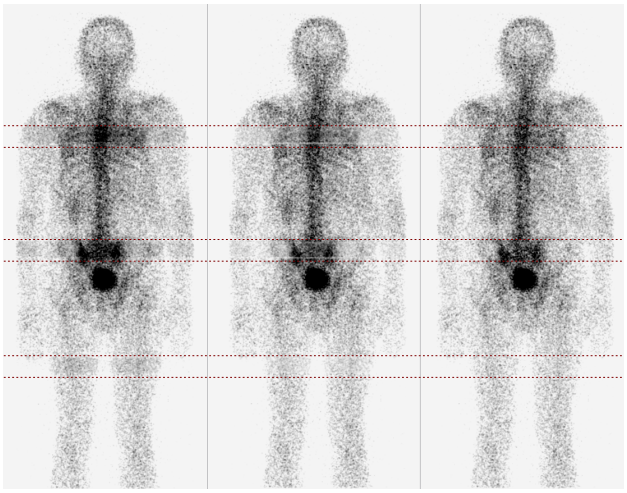

Fig. 4. Image stitching techniques performed before reconstruction. Left: average, Middle: cross-fade, Right: our method. Note the stitching effect at overlapping regions on average and cross-fade stitched images.

The first question was answered by inspecting the stitched projection series and their corresponding reconstructed whole body SPECT. All cases were classified as accepted or not accepted and the acceptance ratio was determined. The non-reconstructed but stitched series were inspected as well and compared to known stitching methods such as average or cross-fade (see Fig. 4).

The second question was answered by checking all reconstructed whole body SPECT images and their corresponding artificial planar images. During the check the physicians were seeking for hot spots over the axial slices of the WB SPECT that could not be located on the corresponding artificial planar images.

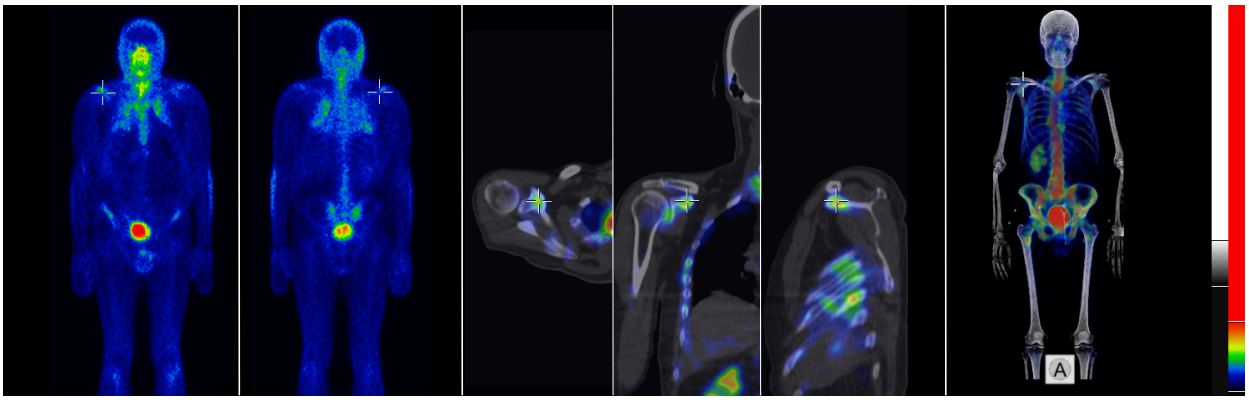

Fig. 5. Example layout for evaluating our whole body SPECT studies. First two images show the artificial anterior - posterior image pairs. Middle three images show the axial-sagittal-coronal views of the fused whole body SPECT-CT. Last image shows the volume rendering view of the fused whole body SPECT-CT. Note the synchronized cursor position representing a hotspot in the shoulder.

TABLE II
SCORING RESULTS OF STITCHING METHODS

Stitching methods	Acceptance ratio
Average	7%
Cross-fade	43%
Our method	99%

III. RESULTS

For the acceptance ratio of average, cross-fade and our method see Tab. II.

The planar image projections did not include noticeable stitching artifacts based on our method and they appeared to be a useful aid for fast localization during the evaluation. For an example layout of the evaluation see Fig. 5.

IV. CONCLUSIONS AND FUTURE WORKS

A. Conclusions

We have proposed a new SPECT-CT acquisition workflow with a novel stitching algorithm to provide whole body SPECT images for bone scans. The difference comparing to the gold standard workflows appears on two levels:

On one hand we do not acquire planar scans at all, but in return we acquire SPECT scans that are stitched to a whole body SPECT before reconstruction. Our stitching method is very accurate and fully automated due to the approach of stitching before reconstruction on the level of projections. We derive artificial planar images from the reconstructed SPECT to aid localization during evaluation.

On the other hand the overall time to acquire a SPECT scan series covering the whole body takes average 16 minutes which is comparable to present gold standard workflows including a planar scan pair and an additional SPECT in 45-60 minutes.

This approach can significantly decrease the time to perform a bone scan in the daily routine which helps maximizing the number of scans per day.

B. Future Works

We will focus on minimizing the the overlapping size of the SPECT scans to further increase the overall range of the bone scan. At the same time we will investigate the feasibility of building the handling of overlapping information into the reconstruction itself. On the long term we will investigate how the reconstruction quality could be preserved while further decreasing the number of projections and time of the acquisition per projection. We will collect a larger amount of clinical data for further tests and validation. We will especially focus on the investigation of those cases when hot spots lay in the stitched area.

REFERENCES

[1] E. E. Sapir, U. Metser, E. Mishani, et al., The Detection of Bone Metastases in Patients with High-Risk Prostate Cancer: 99mTc-MDP Planar Bone Scintigraphy, Single- and Multi-Field-of-View SPECT, 18F-Fluoride PET, and 18F-Fluoride PET/CT, *Journal of Nuclear Medicine*, vol. 47, 2006, pp 287-297.

[2] H. Schirrmeister, G. Glatting, J. Hetzel, et al., Prospective Evaluation of the Clinical Value of Planar Bone Scans, SPECT, and 18F-Labeled NaF PET in Newly Diagnosed Lung Cancer *Journal of Nuclear Medicine*, vol. 42, 2001, pp. 1800-1804.

[3] L. J. Han, T. K. Au-Yong, W. C. M. Tong, et at., Comparison of bone single-photon emission tomography and planar imaging in the detection of vertebral metastases in patients with back pain, *Eur. J Nucl Med Mol Img*, vol. 25, 1998, pp. 635-638.

[4] E. Leung, R. Wassenaar, X. Pham, et al., Prospective comparison of whole body SPECT with traditional planar bone scans, *J Nucl Med.*, vol. 49,2008, 8P.

[5] O. Schillaci, Hybrid SPECT/CT: a new era for SPECT imaging?, *Eur. J. Nucl. Med. Mol. Img.*, vol. 32, 2005, pp. 521-524.

[6] O. Mawlawi, W. Erwin, T. Pan, et al., What is the optimal minimum whole body bone SPECT scan duration that can replace planar bone scintigraphy?, *J Nucl Med.*, vol. 48, 2007, 120P

[7] A. Szlavecz, B. Benyo, G. Hesz, T. Bukki, An Optimized SPECT Reconstruction Algorithm with Attenuation Correction and Resolution Recovery, *CARS Computer Assisted Radiology and Surgery, Berlin*, 2009.

[8] A. Szlavecz, G. Hesz, T. Bukki, et al., GPU-Based Acceleration of the MLEM Algorithm for SPECT Parallel Imaging with Attenuation Correction and Compensation for Detector Response, *Proceedings of the 18th International Federation of Automatic Control (IFAC) World Congress*, 2011, pp. 6195-6200.

[9] M. J. Berger, J. S. Coursey, M. A. Zucker, et al., Stopping-Power and Range Tables for Electrons, Protons, and Helium Ions, *http://www.nist.gov/pml/data/star/index.cfm*, 2009.